Electrical network of nanofluidic diodes in electrolyte solutions: connectivity and coupling to electronic elements

Vicente Gomez,[1] Javier Cervera,[2] Saima Nasir,[3,4] Mubarak Ali,[3,4] Wolfgang Ensinger,[3] Salvador Mafe,[2] and Patricio Ramirez[1,*]

[1]Dept. de Física Aplicada, Universitat Politècnica de València, E-46022 València, Spain.

[2]Dept. de Física de la Tierra i Termodinàmica, Universitat de València, E-46100 Burjassot, Spain.

[3]Dept. of Material- and Geo-Sciences, Materials Analysis, Technische Universität Darmstadt, D-64287 Darmstadt, Germany

[4]Materials Research Department, GSI Helmholtzzentrum für Schwerionenforschung, Planckstrasse 1, D-64291, Darmstadt, Germany

*Corresponding author. *Email address*: patraho@fis.upv.es (P. Ramirez)

Abstract

We consider a nanopore network with simple connectivity, demonstrating a two-dimensional circuit (full-wave rectifier) with ensembles of conical pores acting as nanofluidic diodes. When the bridge nanopore network is fed with an *input* potential signal of fluctuating polarity, a fixed *output* polarity is obtained. The full-wave rectification characteristics are demonstrated with square, sinusoidal, and white noise input waveforms. The charging of a load capacitor located between the two legs of the bridge demonstrates that the nanofluidic network is effectively coupled to this electronic element. These results can be relevant for energy transduction and storage procedures with nanopores immersed in electrolyte solutions. Because the individual nanofluidic resistances can be modulated by chemical, electrical, and optical signals, the balanced bridge circuit can also be useful to miniaturize nanopore-based sensing devices.

Keywords: nanopore, electrolyte solution, fluctuating signal, full wave rectifier

1. Introduction

The rich diversity of biological ion channels is crucial for the cell membrane selectivity to different chemical species and for information processing with neural networks.[1] Pore-based biomimetic nanostructures operating in electrolyte solutions can show some of these functional characteristics,[2-5] which are potentially useful for sensing, drug controlled release, and energy conversion and storage.[6-8] However, it is not obvious to what extent the nanopores can be connected in networks capable of performing collective tasks. Moreover, the nanopore networks should be effectively coupled to conventional electronic elements such as capacitors to achieve the full functionality required for sensors and bioelectronic interfaces operating in electrolyte solutions.[6,7]

We have demonstrated previously[9] that a nanofluidic diode can provide a significant rectification of white noise signals (electric potentials of zero average). Due to the biomimetic nature of this single pore, the results have also clear implications for wide ion channels formed by proteins reconstituted on planar lipid bilayers.[10] We consider here a network with simple connectivity, demonstrating two-dimensional arrangements such as a full-wave rectifier of external fluctuating signals (Figure 1). The four multipore membranes with conical nanopores act as potential dependent resistances when the electrical network forming the bridge rectifier is fed with periodic and fluctuating potentials. Regardless of the input potential polarity, a fixed output potential polarity is obtained when the individual nanofluidic diodes are connected to one another. The full-wave rectification characteristics are demonstrated with different input potential waveforms (square wave, sinusoidal, and white noise signals). A load capacitor can also be connected between the two legs of the bridge (Figure 1), with the voltmeter measuring the output potential. The charging of the central capacitor demonstrates that the nanofluidic network is effectively coupled to this electronic element: the alternating potentials are converted into unidirectional currents and the capacitor is charged to a maximum voltage. Remarkably, because the individual nanofluidic resistances in the membranes of Figure 1 can be externally

tuned by chemical, electrical, and optical input signals (see Reference [4] and references therein), the above networks can also be employed in nanopore-based sensing devices.

2. Experimental methods

Nanopore fabrication. Polyethylene terephthalate (PET) polymer foils (Hostaphan RN 12, Hoechst) of thickness 12 μm are irradiated with 10^4 swift heavy (Au) ions cm^{-2} of energy of 11.4 MeV per nucleon (UNILAC linear accelerator, GSI, Darmstadt). The resulting conical multipore membranes are prepared by using asymmetric track-etching methods.[11] The conical pores have radii in the ranges 10 – 20 nm for the tip side and 100 – 200 nm for the base side, as estimated from the measured steady-state current (I) – potential (V) curves.[12] The etching process gives carboxylate residues on the pore wall surface. These groups are ionized at pH = 7, being responsible for the nanofluidic diode rectification[13] (control experiments at pH = 3, neutral pore, give no rectification[9]). The pH value is checked before and after each measurement by using a Crison GLP22 pH-meter.

Electrical Measurements. The Ag|AgCl electrodes immersed in the bathing solutions are used to apply the fluctuating input potentials as well as to measure the potential drops in the fluidic circuit. The observed electrical rectification is due to the pore charge asymmetry: the current that enters the cone tip (high charge density) experiences an electrical resistance lower than the current entering the wide basis (low charge density).[12] The $I – V$ curves are measured using a picoammeter/voltage source (Keithley 6487/E) and the voltage across the capacitor is measured using a multimeter (Keithley 2000/E).

3. Results and Discussion

Figure 1 shows the electrochemical scheme of the nanopore-based bridge acting as a full-wave rectifier. A capacitor of capacitance *C* can also be connected between the bridge legs *c* and *d*. All pores are immersed in KCl aqueous solutions of concentration c_0 = 0.1 M and *pH* = 7.

Figure 2 shows the individual steady-state current (*I*)–voltage (*V*) curves for the four membranes of Figure 1. Each curve was measured several times in order to check the reproducibility of the results. The nanopore rectification characteristics depend on the electrolyte concentration and can be optimized at intermediate values of the order of c_0 = 0.1 M.[12,13]

Figure 3a shows a scheme of the open diode circuit equivalent to the fluidic circuit of Figure 1. Figure 3b corresponds to the open circuit steady-state current (I_{in})–voltage (V_{in}) curve for the complete full-wave rectifier. The *s*-shaped curve reflects the dominant role of the reverse-polarized nanofluidic diode in each branch of the curve. Figure 3c shows a scheme of the short circuit. Figure 3d corresponds to the steady-state current (I_{sc})–voltage (V_{in}) curve for the short circuit. The electric current is rectified in the whole range of applied voltages (the small, negative values observed for the low, positive values of V_{in} resulted from the asymmetry of the electrodes.) The curves in Figures 3b and 3d are not perfectly symmetrical because the nanofluidic membrane diodes of Figure 2 are not identical.

Figure 4 shows the input potential $V_{in}(t)$ and current $I_{in}(t)$, together with the output potential $V_{out}(t)$, for the sinusoidal (a), square wave (b), and white noise (c) signals. A voltmeter measuring $V_{out}(t)$ is now connected between the two legs *c* and *d* of Figure 1. The fluctuating input potential $V_{in}(t)$ of amplitude V_0 is externally applied in the Ag|AgCl electrodes, giving a time (*t*) dependent electric current $I_{in}(t)$. For the low frequency signals used,[9,10,14] $I_{in}(t)$ is slave of $V_{in}(t)$. (Note that the period of the potential is much longer than the relaxation time in the small solution volumes characteristic of nanopores and ion channels.[10]) The results shown in

Figure 4 confirm further the full wave characteristics of the nanofluidic network for the case of three different time-dependent signals.

The maximum current which can be achieved in the above experimental schemes scales with the effective membrane area, which is proportional to the exposed membrane area (1 cm^2 approximately). As to the maximum voltage, it is influenced by the electrodes used (voltages above 4 V and currents of the order of 0.1 mA can be measured safely without a noticeable loss of functionality of the electrodes. Finally, concerning the frequency response, the operation limit is marked by the rectification ratio required for the full wave rectifier function to be operative. In preliminary experiments, significant membrane rectification ratios were observed up to frequencies close to 1 kHz, which could be then considered as an upper bound.

Figure 5a-c show the capacitor voltage *vs* time charging curves for the different signals of Figure 4. Because of the full-wave rectification, significant capacitor charging can be achieved, leading to the saturation voltage $V_C(t \to \infty) \equiv V_C(\infty)$ at long enough times.[9] In particular, Figure 5 shows that the square wave input signal gives the maximum output capacitor voltage, which is of the order of 1 V within 1 min only. As it could be expected, an increase in the capacitance C yields more stable output potentials $V_C(\infty)$. Because the resistances of the multipore membranes are of the order of 10 kΩ (see Figure 2), the effective charging time for the equivalent *RC* circuit is of the order of 10 s for C = 1 mF and increase linearly with C, in agreement with the experimental curves of Figure 5. These facts confirm further the effective coupling between the nanofluidic membrane diodes and the capacitor.

The results of Figures 3 and 4 demonstrate that full wave rectification can be achieved with conical nanopores. The efficient connectivity between pores defined at the nanoscale and conventional electronic elements produces a prescribed collective response. This electrical functionality is potentially useful for electrochemical devices where electronic components (load capacitors here) are used together with the electrolyte solutions characteristic of living systems. Figure 5 indicates also that significant energy conversion from an *input* fluctuating signal (an

external potential here) can be realized with the multipore-based circuit. We have demonstrated recently this energy transduction using a half-wave rectification scheme based on a single nanopore.[9] Figure 5 demonstrates that this result can be scaled up significantly using a full-wave rectification scheme based on an arrangement of multipore membranes working in concert. The new experimental scheme allows a significant increase in the charging currents and the energy stored.

Note finally that the artificial nanopores used here show some of the characteristics (e.g. ionic selectivity and rectification) of the ion channels inserted in typical biological membranes operating in aqueous salt solutions.[1] The experiments suggest methods to quantify the accumulative effects caused by low frequency external signals at a more fundamental level than the traditional tissue scale using biological channels instead of artificial nanopores.

4. Conclusions

We have designed and characterized a simple network of multipore membranes with nanofluidic diodes capable of performing collective tasks (full-wave rectification) when connected to conventional electronic elements. The results suggest that basic circuits of soft matter nanostructures can be electrically coupled to these macroscopic elements in energy transduction with electrochemical cells, nanopore-based sensors, and bioelectronics interfaces operating in electrolyte solutions. This is also the case of microdroplets with incorporated protein diodes.[15] We have used multipore membranes to achieve the high outputs required in real operating conditions (the basic ideas involved have previously been demonstrated using a single nanopore[9]).

Portable microchip units are currently available.[6,16,17] While we have not addressed here the integration of the network in miniaturized chips, the basic electrochemical concepts involved are well-established and the experimental results are robust enough to suggest that this integration should be feasible. Potential applications are the detection of chemical, electrical or optical

inputs that could modify the individual nanofluidic resistances balancing the bridge network and the feeding of a microdevice or external circuitry using the energy stored in the capacitor.

Acknowledgements

We acknowledge the support from the Ministry of Economic Affairs and Competitiveness and FEDER (project MAT2015-65011-P) and the Generalitat Valenciana (project Prometeo/GV/0069 for Groups of Excellence). M.A., S.N. and W.E. acknowledge the funding from the Hessen State Ministry of Higher Education, Research and the Arts, Germany, under the frame of LOEWE project iNAPO.

References

[1] B. Hille, Ionic Channels of Excitable Membranes (Sinauer Associates Inc., Sunderland, MA, 1992).

[2] C. R. Martin, Z. S. Siwy, *Science* **2007,** *317*, 331.

[3] X. Hou, L. Jiang. Learning, *ACS Nano* **2009,** *3*, 3339.

[4] P. Ramirez, J. Cervera, M. Ali, W. Ensinger, S. Mafe, *ChemElectroChem* **2014,** *1*, 698.

[5] G. Pérez-Mitta, J. S. Tuninetti, W. Knoll, C. Trautmann, M. E. Toimil-Molares, O. Azzaroni, *J. Amer. Chem. Soc.* **2015,** *137*, 6011.

[6] M. Tagliazucchi, I. Szleifer, *Mater. Today* **2015,** *18*, 131.

[7] N. Misra, J. A. Martinez, S.-C. J. Huang, Y. Wang, P. Stroeve, C. P. Grigoropoulos, A. Noy, *Proc. Natl. Acad. Sci. U.S.A.* **2009,** *106*, 13780.

[8] Y. Hou, R. Vidu, P. Stroeve, *Ind. Eng. Chem. Res.* **2011,** *50*, 8954.

[9] V. Gomez, P. Ramirez, J. Cervera, S. Nasir, M. Ali, W. Ensinger, S. Mafe, *Sci. Rep.* **2015,** *5*, 9501.

[10] M. Queralt-Martin, E. Garcia-Gimenez, V. M. Aguilella, P. Ramirez, S. Mafe, A. Alcaraz, *Appl. Phys. Lett.* **2013,** *103*, 043707.

[11] P. Apel, *Radiat. Meas.* **2001,** *34*, 559.

[12] J. Cervera, B. Schiedt, R. Neumann, S. Mafe, P. Ramirez, *J. Chem. Phys.* **2006,** *124*, 104706.

[13] J. Cervera, P. Ramírez, J. A. Manzanares, S. Mafé, *Microfluid. Nanofluid.* **2010,** *9*, 41.

[14] D. Momotenko, H. H. Girault, *J. Am. Chem. Soc.* **2011,** *133*, 14496.

[15] G. Maglia, A. J. Heron, W. L. Hwang, M. A. Holden, E. Mikhailova, Q. Li, S. Cheley, H. Bayley, *Nat. Nanotechnol.* **2009,** *4*, 437.

[16] S. Senapati, S. Basuray, Z. Slouka, L.-J. Cheng, H.-C. Chang, *Top Curr Chem.* **2011,** *304*, 153.

[17] K. Tybrandt, R. Forchheimer, M. Berggren, *Nat. Commun.* **2012,** *3*, 871.

Figure captions

Figure 1

Scheme of the experimental set-up showing the membrane-based bridge acting as a full-wave rectifier and the measuring output voltmeter. The numbers denote the different nanoporous membrane samples. A capacitor of capacitance C (not shown here) can be connected between the points c and d in the scheme. The colors of electrodes indicate the different electrical polarity at time $t = 0$.

Figure 2

The individual steady-state current (I)–voltage (V) curves for the four multipore membranes of Figure 1. The results are obtained for $pH = 7$ and the electrolyte concentration $c_0 = 0.1$ M KCl.

Figure 3

(a) Scheme of the diode circuit equivalent to the fluidic circuit of Figure 1. (b) Steady-state open circuit current (I_{in})–voltage (V_{in}) curve for the complete full-wave rectifier. (c) Scheme of the short diode circuit (d) Steady-state short circuit current (I_{sc})–voltage (V_{in}) curve for the complete full-wave rectifier.

Figure 4

The input potential $V_{in}(t)$ and current $I_{in}(t)$, together with the output potential $V_{out}(t)$, for the sinusoidal (a), square wave (b), and white noise (c) signals.

Figure 5

Capacitor voltage $V_C(t)$ *vs* time charging curves for the input signals of Figure 4. The results correspond to the circuit of Figure 1 for the values of the capacitance indicated in the central curve.

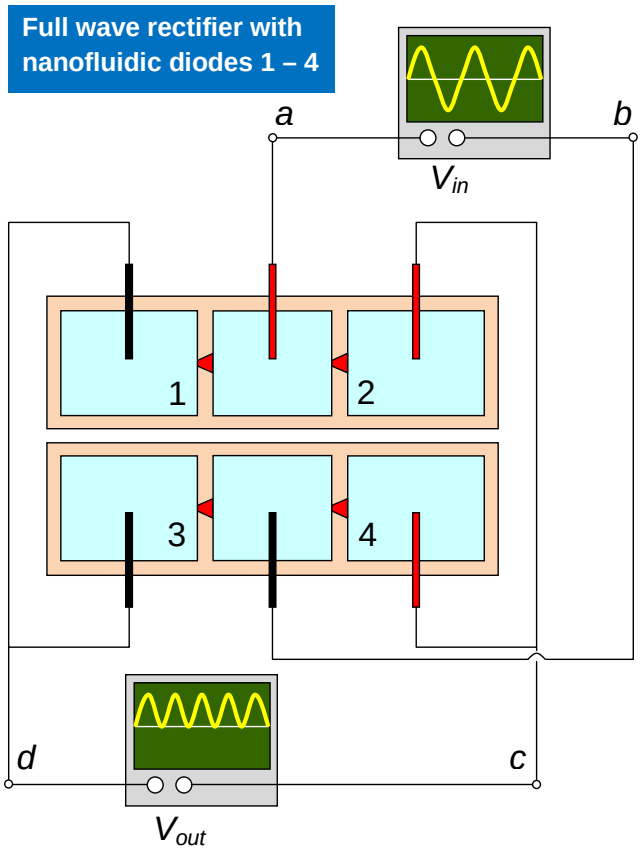
Full wave rectifier with nanofluidic diodes 1 – 4
a
b
V_{in}
1
2
3
4
d
c
V_{out}

Figure 1

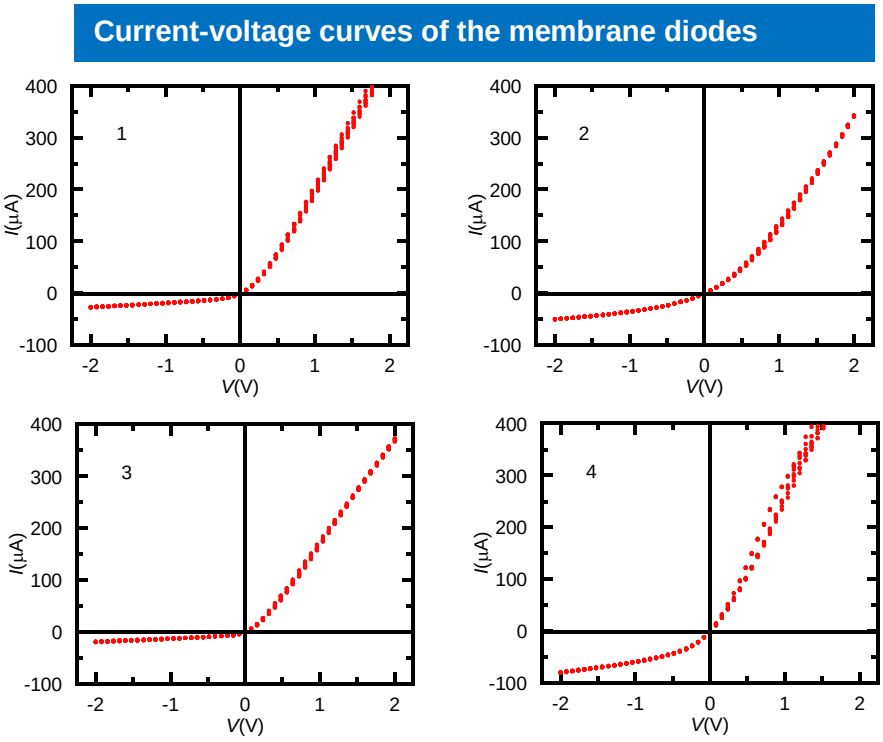
Current-voltage curves of the membrane diodes
1
2
3
4
I(μA)
V(V)
400
300
200
100
0
-100
-2
-1
0
1
2

Figure 2

Current-voltage curve of the full wave rectifier

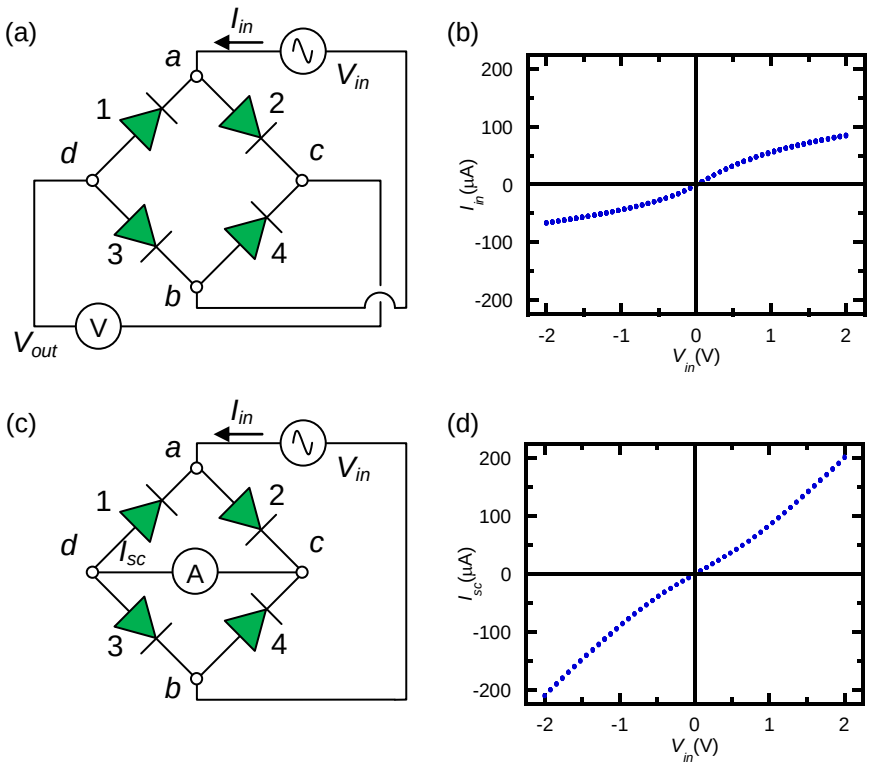

Figure 3

Full-wave rectifying characteristics for thee input signals

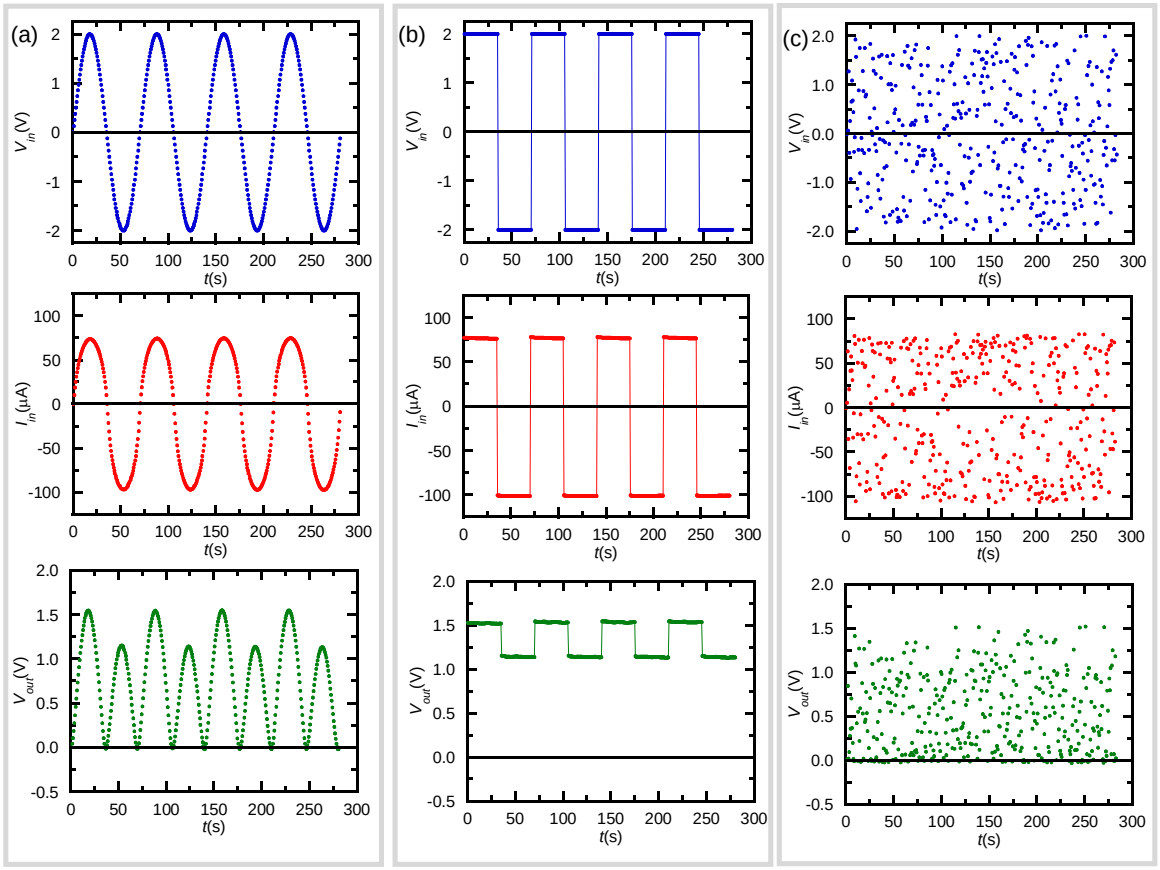

Figure 4

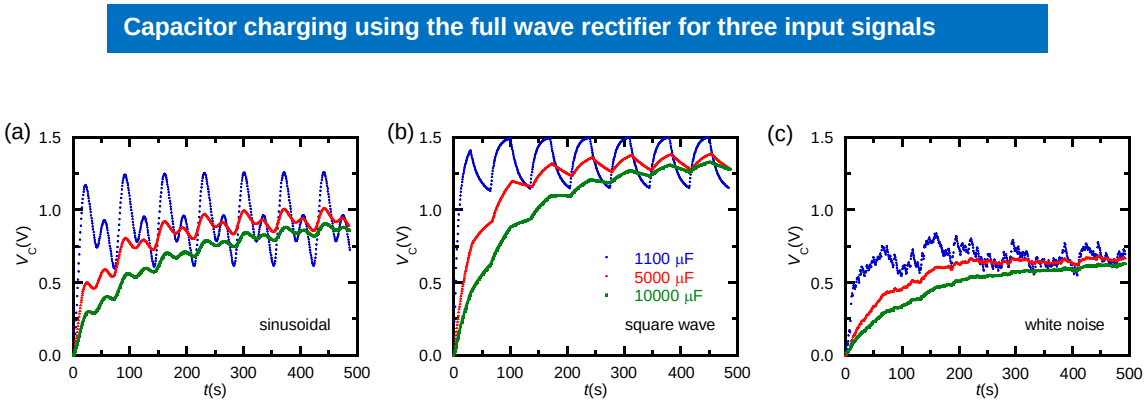
Capacitor charging using the full wave rectifier for three input signals
(a)
(b)
(c)
V_c(V)
t(s)
1100 μF
5000 μF
10000 μF
sinusoidal
square wave
white noise

Figure 5